Missense Mutations in the Human Nanophthalmos Gene *TMEM98* Cause Retinal Defects in the Mouse

Sally H. Cross[1]*, Lisa Mckie[1], Margaret Keighren[1], Katrine West[1], Caroline Thaung[2,3], Tracey Davey[4] and Ian J. Jackson[1]

[1]MRC Human Genetics Unit, MRC Institute of Genetics and Molecular Medicine, University of Edinburgh, Crewe Road, Edinburgh EH4 2XU, United Kingdom

[2]Moorfields Eye Hospital NHS Foundation Trust, 162 City Road, London EC1V 2PD, United Kingdom.

[3]UCL Institute of Ophthalmology, 11-43 Bath Street, London EC1V 9EL, United Kingdom.

[4]Electron Microscopy Research Services, Newcastle University, Newcastle NE2 4HH, United Kingdom.

*corresponding author Email: sally.cross@igmm.ed.ac.uk Tel: +44 131 651 8500

Running Title: *TMEM98* Nanophthalmos Mutations in the Mouse

Grant information: Funded by the MRC University Unit award to the MRC Human Genetics Unit

ABSTRACT

PURPOSE. We previously found a dominant mutation, *Rwhs*, causing white spots on the retina accompanied by retinal folds. Here we identify the mutant gene to be *Tmem98.* In humans, mutations in the orthologous gene cause nanophthalmos. We modelled these mutations in mice and characterised the mutant eye phenotypes of these and *Rwhs*.

METHODS. The *Rwhs* mutation was identified to be a missense mutation in *Tmem98* by genetic mapping and sequencing. The human *TMEM98* nanophthalmos missense mutations were made in the mouse gene by CRISPR-Cas9. Eyes were examined by indirect ophthalmoscopy and the retinas imaged using a retinal camera. Electroretinography was used to study retinal function. Histology, immunohistochemistry and electron microscopy techniques were used to study adult eyes.

RESULTS. An I135T mutation of *Tmem98* causes the dominant *Rwhs* phenotype and is perinatally lethal when homozygous. Two dominant missense mutations of *TMEM98*, A193P and H196P are associated with human nanophthalmos. In the mouse these mutations cause recessive retinal defects similar to the *Rwhs* phenotype, either alone or in combination with each other, but do not cause nanophthalmos. The retinal folds did not affect retinal function as assessed by electroretinography. Within the folds there was accumulation of disorganised outer segment material as demonstrated by immunohistochemistry and electron microscopy, and macrophages had infiltrated into these regions.

CONCLUSIONS. Mutations in the mouse orthologue of the human nanophthalmos gene *TMEM98* do not result in small eyes. Rather, there is localised disruption of the laminar structure of the photoreceptors.

INTRODUCTION

There are a range of genetic disorders which present with a reduced eye size. In microphthalmia the reduced size is associated with additional developmental eye defects, such as coloboma, and may also include developmental defects in other organs. In some cases there is an overall size reduction without developmental defects. These comprise a spectrum of increasing severity termed simple microphthalmia, posterior microphthalmia and nanophthalmos, in which the short axial length results in high hyperopia [1, 2]. Nanophthalmos, in which eye length is reduced by 30% or more, can be associated with other ocular features, notably a thickened choroid and sclera, as well as a high incidence of glaucoma, corneal defects, vascular defects and a range of retinal features including retinitis pigmentosa, retinoschisis, retinal detachments and retinal folds.

A number of genes have been found to be associated with nanophthalmos [2]. Patients with heterozygous or homozygous mutations in the *BEST1* gene can have a range of defects [3]. *BEST1* encodes the bestrophin-1 protein, a transmembrane protein located in the basolateral membrane of the retinal pigment epithelium (RPE) [4]. The predominant disease resulting from mutations in *BEST1* is Best vitelliform macular dystrophy, in which subretinal lipofuscin deposits precede vision defects [5]. These patients in early stages have a normal electroretinogram (ERG) but have a defect in electrooculography (EOG) indicative of a abnormality in the RPE. This can progress to retinitis pigmentosa. Five families have been reported with dominant vitreoretinochoroidopathy and nanophthalmos due to three different missense mutations in *BEST1*. Each mutant allele can produce two isoforms, one containing a missense mutation and one containing an in-frame deletion [6]. Similar rare associations have been seen for mutations in the *CRB1* gene that encodes an apical transmembrane protein important for determining cell polarity in photoreceptors [7]. *CRB1* mutations are most frequently found associated with recessive retinitis pigmentosa or with Leber congenital amaurosis and the disease phenotype observed in patients is very variable suggestive of the influence of genetic modifiers [8, 9]. However, in two cases, both involving consanguineous families, the retinal dystrophy is associated with nanophthalmos [10, 11].

In contrast to *BEST1* and *CRB1*, mutations in three other genes lead to more frequent associations with nanophthalmos. Several families with nanophthalmos have been found to have clear loss of function mutations in both alleles of the gene encoding membrane-type frizzled related protein, *MFRP*, that is expressed principally in the RPE and ciliary body [12].

Homozygous loss of function mutations in *MFRP* have been found in other individuals with posterior microphthalmia plus retinitis pigmentosa, foveoschisis and drusen, indicating likely genetic background effects on the severity or range of the disease [13-15]. A second autosomal recessive nanophthalmos gene is *PRSS56*. encoding a serine protease. Families with biallelic mutations in this gene have been characterised, some of whom have posterior microphthalmia whilst others have nanophthalmos [16-18]. There is no apparent genotype-phenotype correlation; there are patients with homozygous frameshift mutations with either condition. Intriguingly, association of variants at *PRSS56* with myopia has been reported in genome-wide association studies [19, 20].

Most recently three families have been characterised in which heterozygous mutations in *TMEM98* are segregating with nanophthalmos. Two families have missense mutations, the third has a 34bp deletion spanning a splice site which could lead to production of a potentially functional protein with an internal deletion [21, 22]. Caution in assigning a role for *TMEM98* in nanophthalmos has been raised by findings in another study where different heterozygous missense mutations in *TMEM98* were found in patients with high myopia and cone-rod dystrophy [23].

Mouse models with mutations in most of these genes have been analysed. Mice which have targeted disruption of the *Best1* gene do not recapitulate the human bestrophinopathy phenotype or have only an enhanced response in EOG (indicative of a defect in the RPE) [24, 25]. However, when the common human mutation, W93C, is engineered into the mouse gene, both heterozygous and homozygous mice show a distinctive retinal pathology of fluid or debris filled retinal detachments which progress with age [26]. Spontaneous and targeted mutations in mouse *Crb1* have been characterised, and they show similar, though not identical, recessive retinal phenotypes that had variable ages of onset [27-29]. The defects found are focal. Folds and rosettes appear in the photoreceptor layer that are visualised as white patches on retinal imaging. In a complete loss-of-function allele and the frameshift allele $Crb1^{rd8}$ the folds and rosettes are adjacent to discontinuities in the outer (external) limiting membrane (OLM) accompanied by loss of adherens junctions, and within them the photoreceptors, separated from the RPE, show degeneration [27, 28]. In mice engineered to carry a missense mutation, $Crb1^{C249W/-}$, that causes retinitis pigmentosa in humans, although the OLM appears intact, retinal degeneration still occurs, albeit later than in the other models [29]. Similar to the human phenotype the extent of the retinal spotting observed in *Crb1* mutants is strongly affected by the genetic background.

Two lines of mice with spontaneous mutations in *Mfrp* have been described [30-32]. These do not recapitulate the nanophthalmic phenotype observed in humans. Instead both have the same recessive phenotype of white spots on the retina, which correlate with abnormal cells below the retina that stain with macrophage markers, and progress to photoreceptor degeneration. For the *Mfrp*^{rdx} mutation, atrophy of the RPE was reported [31] and for *Mfrp*^{rd6} a modest ocular axial length reduction from about 2.87 to 2.83 mm was reported although apparently not statistically significant [33]. A screen for mice with increased intraocular pressure (IOP) found a splice mutation in the *Prss56* gene predicted to produce a truncated protein [17]. The increased IOP was associated with a narrow or closed iridocorneal angle, analogous to that seen in human angle closure glaucoma. In addition these mice have eyes that are smaller than littermates, although the size reduction is variable and slight, ranging from 0 to 10% decrease in axial length. Reduction in axial length only becomes statistically significant after post-natal day seven. More recently it has been shown that mice deficient for *Prss56* have eyes with a decreased axial length and hyperopia [34].

To date no mouse models of *TMEM98* have been reported. We describe here characterisation of a mouse mutation in *Tmem98*, which results in a dominant phenotype of retinal folds and rosettes. In addition we engineer the two nanophthalmos-associated missense mutations of *TMEM98* into the mouse gene and show that these mice also, when homozygous or when compound heterozygous, have the same retinal fold and rosette phenotype.

MATERIALS AND METHODS

Mice

All mouse work was carried out in compliance with UK Home Office regulations under a UK Home Office project licence and experiments adhered to the ARVO Statement for the Use of Animals in Ophthalmic and Vision Research. Clinical examinations were performed as previously described [35]. Fundus imaging was carried out as described [36]. Mice carrying a targeted knockout-first conditional-ready allele of *Tmem98, Tmem98*$^{tm1a(EUCOMM)Wtsi}$ (hereafter *Tmem98*^{tm1a}), were obtained from the Sanger Institute [37]. *Tmem98*$^{tm1a/+}$ mice were crossed with mice expressing Cre in the germ-line to convert this 'knockout-first' allele to the reporter knock-out allele *Tmem98*$^{tm1b(EUCOMM)Wtsi}$ (hereafter *Tmem98*^{tm1b}). In this allele the DNA between the loxP sites in the targeting cassette which includes the neo selection gene and

the critical exon 4 of *Tmem98* is deleted. To create the *Tmem98*^{H196P} allele the CRISPR design site www.crispr.mit.edu was used to design guides and the selected guide oligos ex7_Guide1 and ex7_Guide2 (Table 1) were annealed and cloned into the *Bbs I* site of the SpCas9 and chimeric guide RNA expression plasmid px330 [38] (pX330-U6-Chimeric_BB-CBh-hSpCas9 was a gift from Feng Zhang (Addgene plasmid #42230, https://www.addgene.org/)). Following pronuclear injection of this plasmid along with repair oligo H196P (Table 1) the injected eggs were cultured overnight to the 2-cell stage and transferred into pseudopregnant females. To create the *Tmem98*^{A193P} allele Edit-R crRNA (sequence 5'- CCAAUCACUGUCUGCCGCUG-3') (Dharmacon) was annealed to tracrRNA (Sigma) in IDT Duplex buffer (IDT). This, along with Geneart Platinum Cas9 nuclease (Invitrogen B25641) and repair oligo A193P (Table 1) were used for pronuclear injection as described above. Pups born were screened for the targeted changes by sequencing PCR fragments generated using the oligos ex7F and ex7R (Supplementary Table S1) and lines established carrying the targeted missense mutations. Genotyping was initially done by PCR, and sequencing where appropriate, using the primers in Supplementary Table S1. Subsequently most genotyping was performed by Transnetyx using custom designed assays (http://www.transnetyx.com). All lines were maintained on the C57BL/6J mouse strain background.

DNA Sequencing

The candidate interval was captured using a custom Nimblegen array and sequenced with 454 technology by Edinburgh Genomics (formerly known as GenePool) (http://www.genomics.ed.ac.uk).

Electroretinography

All electroretinography was carried out according to International Society for Clinical Electrophysiology of Vision guidelines. Prior to electroretinography mice were dark adapted overnight (>16 hours) and experiments were carried out in a darkened room under red light using an HMsERG system (Ocuscience). Mice were anesthetised using isofluorane and their pupils dilated by the topical application of 1% w/v tropicamide. Three grounding electrodes were placed subcutaneously (tail, and each cheek) and silver embedded electrodes were positioned on the corneas using hypromellose eye drops (2.5% methylcellulose coupling agent) held in place with a contact lens. Animals were kept on a heated platform to maintain them at 37°C and monitored using a rectal thermometer. A modified QuickRetCheck (Ocuscience) protocol was used for obtaining full-field scotopic

ERGs. Briefly, 4 flashes at 10 mcd.s/m^2 at 2 s intervals were followed by 4 flashes at 3 cd.s/m^2 (at 10 s intervals) and then 4 flashes at 10 cd.s/m^2 (at 10 s intervals).

Histology and Immunostaining

Mice were culled, eyes enucleated and placed into Davidson's fixative (28.5% ethanol, 2.2% neutral buffered formalin, 11% glacial acetic acid) for 1 hour (cryosectioning) or overnight (wax embedding) except for the eye used for Fig. 1 which was placed in 10% neutral buffered formalin for 24 hours before immersion in Davidson's fixative. Prior to wax embedding eyes were dehydrated through an ethanol series. Haematoxylin and eosin staining was performed on 5 or 10 µm paraffin embedded tissue sections and images captured using a Nanozoomer XR scanner (Hamamatsu) and viewed using NDP.view2 software. For cryosectioning, fixed eyes were transferred to 5% sucrose in PBS and once sunk transferred to 20% sucrose in PBS overnight. Eyes were then embedded in OCT compound and cryosectioned at 14 µM. For immunostaining on cryosections, slides were washed with water then PBS and post-fixed in acetone at -20°C for 10 minutes. They were then rinsed with water, blocked in 10% DS, 0.1% Tween-20 in TBS (TBST) for one hour and then incubated with primary antibodies diluted in TBST with 5% DS for two hours at room temperature or overnight at 4°C. Subsequently, after washing with TBST, the slides were incubated with Alexa Fluor secondary antibodies (Invitrogen) diluted 1:400 in TBST with 5% DS at room temperature for one hour. Following washing with TBST coverslips were mounted on slides in Prolong Gold (ThermoFisher Scientific) and confocal images acquired on a Nikon A1R microscope. Images were processed using either NIS-Elements or ImageJ software.

Antibodies

Primary antibodies used are listed in Table 2. DNA was stained with TOTO-3 (Invitrogen) or 4',6-Diamidine-2'-phenylindole dihydrochloride (DAPI).

Transmission Electron Microscopy

Samples were fixed in 2% EM grade glutaraldehyde (TAAB Laboratory Equipment, Aldermaston, UK) in sodium cacodylate buffer at 4°C overnight, post-fixed in 1% osmium

tetroxide (Agar Scientific , Essex, UK), dehydrated in increasing concentrations of acetone and impregnated with increasing concentrations of epoxy resin (TAAB Laboratory Equipment). Embedding was carried out in 100% resin at 60°C for 24 hours. Semi-thin survey sections of 1 µm, stained with toluidine blue, were taken to determine relevant area. Ultrathin sections (approximately 70 nm) were then cut using a diamond knife on a Leica EM UC7 ultramicrotome (Leica, Allendale, NJ, USA). The sections were stretched with chloroform to eliminate compression and mounted on Pioloform-filmed copper grids (Gilder Grids, Grantham UK). To increase contrast the grids were stained with 2% aqueous uranyl acetate and lead citrate (Leica). The grids were examined using a Philips CM 100 Compustage (FEI) Transmission Electron Microscope. Digital images were collected using an AMT CCD camera (Deben UK Ltd., Suffolk, UK).

Statistics

For the data shown in Figure 3 an unpaired t test with Welch's correction was performed. For the data shown in Tables 3, S2 and S3 chi square tests were performed using http://graphpad.com/quickcalcs. A value of $P<0.05$ was considered significant.

RESULTS

Rwhs is a missense mutation of the *Tmem98* gene

The *N*-ethyl-*N*-nitrosourea (ENU)-induced mouse mutation retinal white spots (*Rwhs*) was found in a screen for dominant eye mutations [35]. Mice heterozygous for the mutation have white patches on retinal imaging, apparently corresponding to folds or invaginations of the photoreceptor layers (Fig. 1A-B). Initial mapping indicated that *Rwhs* was located within an 8.5 Mb region of chromosome 11 [35]. The retinal phenotype was found on a mixed Balb/c and C3H background. When *Rwhs* mutant mice were backcrossed to the C57BL/6J strain to refine the genetic mapping, some obligate heterozygous mice had retinas with a normal appearance, indicating that the dominant *Rwhs* phenotype is not completely penetrant and that modifiers in the C57BL/6J strain can attenuate it (Supplementary Fig. S1A-D). Crossing *Rwhs* to the wild-derived CAST strain restored the retinal phenotype (Supplementary Fig. S1E-F). Intercrossing of heterozygous mice produced no homozygous offspring at weaning, whereas at late gestation (E17.5-E18.5) fetuses of the three expected genotypes were present at Mendelian ratios indicating that homozygous *Rwhs* is perinatally lethal (Table 3)

(an initial report suggesting that homozygous *Rwhs* mice were viable was incorrect and due to mapping errors [35]). We mapped this lethal phenotype by intercrossing recombinant animals and refined the critical interval to a 200 kb region between the single nucleotide polymorphism markers rs216663786 and rs28213460 on chromosome 11. This region contains the *Tmem98* gene and parts of the *Myo1d* and *Spaca3* genes. We amplified and sequenced all the exons and flanking regions from this region from *Rwhs* mutant mice along with controls. In addition we captured and sequenced all genomic DNA in the candidate interval. We found only a single nucleotide change in the mutant strain compared to the strain of origin, a T to C transition, in exon 5 of *Tmem98* (position 11:80,817,609 Mouse Dec. 2011 (GRCm38/mm10) Assembly (https://genome.ucsc.edu/)) (Fig. 1C). This mutation leads to the substitution of the non-polar aliphatic amino acid, isoleucine, by the polar amino acid threonine (I135T, numbering from entry Q91X86, http://www.uniprot.org). We also investigated the effect of loss-of-function of *Tmem98*. Heterozygous loss-of-function mice are viable and fertile and have normal retinas (Fig. S6D and F). Matings of heterozygous mice carrying the "knock-out first" *Tmem98*^{tm1a} allele produced no homozygous offspring (Supplementary Table S2) demonstrating that loss-of-function of *Tmem98* is lethal. At E16.5-E17.5 the three expected genotypes were present at Mendelian ratios (Supplementary Table S2) and in one litter collected at birth there were three homozgyotes and three wild-types indicating that lethality occurs perinatally.

TMEM98 is a 226 amino acid protein annotated with a transmembrane domain spanning amino acids 4-24 close to the N-terminus (http://www.ensembl.org). It is highly conserved across species; mouse and human TMEM98 share 98.7% amino acid identity and between mouse and *Ciona intestinalis*, the closest invertebrate species to the vertebrates, there is 38.6% amino acid identity in which I135 is conserved (Supplementary Fig. S2). *TMEM98* is widely expressed and is reported to be most highly expressed in human and mouse RPE (http://www.biogps.org). We confirmed its high expression in the RPE and, within the retina, we also find expression at a lower level in the ganglion cell layer (Fig. 1D). The protein has been reported to be a single-pass type II transmembrane protein in which the C-terminal part is extracellular [39].

The Human Nanophthalmos Missense Mutations Cause a Retinal Phenotype in the Mouse

Three mutations in *TMEM98* have been implicated in autosomal dominant nanophthalmos in human families [21, 22]. Two are missense mutations, A193P and H196P. The third is a 34 bp deletion spanning the exon 4/intron 5 boundary [22]. The effect of this on splicing of the *TMEM98* mRNA is unknown, but if the deletion leads to the 132 bp exon 4 being skipped then an aberrant protein with a 44 amino acid internal deletion would be produced. Both missense mutations affect amino acids that are highly conserved (Supplementary Fig. S2) and introduce a proline in the final α-helix of the protein which would likely lead to disruption of the secondary structure of the protein.

To investigate the effect of the two missense mutations we used CRISPR-Cas9 to introduce A193P and H196P into the mouse gene and established lines carrying each. Western blot analysis using a validated anti-TMEM98 antibody (Supplementary Fig. S3A) showed that the mutant proteins are expressed (Supplementary Fig. S3B). Heterozygous mice for both missense mutations were viable and fertile and did not exhibit any gross eye or retinal defects when examined between 5-9 months of age (Supplementary Fig. S4, $Tmem98^{A193P/+}$, n=10; $Tmem98^{H196P/+}$, n=19). In contrast to the $Tmem98^{I135T}$ and knock-out alleles, homozygotes for both the $Tmem98^{A193P}$ and $Tmem98^{H196P}$ alleles were viable and found at the expected Mendelian ratios (Supplementary Table S3). The eyes of homozygous and compound heterozygous mice do not appear to be significantly different in size when compared to wild-type eyes (Fig. 2A). From about 3 months of age we found that white patches developed on the retinas of the homozygous mice and on histological examination we found folds or invaginations in the retinal layers (Fig. 2B). The appearance of the white patches was progressive; at younger ages the retinas of some homozygous mice appeared normal with patches becoming apparent as they aged (Supplementary Fig. S5). In the A193P line only 6 of 7 homozygotes were found to have retinal defects at 6 months of age; the seventh developed white patches on the retina by 9 months. In the H196P line 4/20 homozygous mice that were examined between 3 and 3.5 months of age appeared to have normal retinas. We crossed the lines together to generate compound heterozygotes. $Tmem98^{A193P/H196P}$ (n=4) mice also displayed a similar phenotype of white patches on the retina (Fig. 2B). We also crossed $Tmem98^{H196P}$ mice with mice carrying a loss-of-function allele $Tmem98^{tm1b}$. Compound heterozygous mice were viable and of 17 mice examined all had normal retinas except for one mouse which had three faint spots on one retina at 1 year of age (Supplementary Fig. S6). These results suggest that a threshold level of the mutant missense $TMEM98^{H196P}$ and $TMEM98^{A193P}$ proteins is required to elicit the formation of white

patches on the retina and that the missense mutations found in the human nanophthalmos patients are not loss-of-function.

To assess retinal function electroretinography was carried out on *Tmem98*$^{H196PT/H196P}$ mice and controls at 6 months of age (Fig. 3). There was no significant difference in the a-wave amplitudes between the wild-type and mutant mice.

Characterisation of the Retinal Folds Caused by the A193P and H196P Mutations

We investigated the retinal folds by immunostaining of retinal sections. We found that in the interior of retinal folds the outer segment layer is massively expanded as demonstrated by positive staining for the transmembrane protein prominin-1 and the rod and cone opsins (rhodopsin and ML opsin), indicating that the folds are filled with excess, disorganised outer segments or remnants of outer segments (Fig. 4).

The retinal folds and rosettes seen in other mutant mouse lines are accompanied by defects in the OLM. This structure is formed by adherens junctions between the Müller glia cells and the photoreceptors. We investigated the integrity of the OLM in our mutant mice by staining for β-catenin (Fig. 5A-D). In control mice and in the regions of the retinas of mutant mice unaffected by folds the OLM appeared intact. However, at the folds the OLM is clearly disrupted and gaps can be seen suggesting that cell-cell connections have been broken. Reactive gliosis indicated by upregulation of GFAP in the Müller cells is a response to retinal stress, injury or damage [40]. We observed abnormal GFAP staining in the mutant retinas that was confined to the regions with folds, indicating that in these areas, but not elsewhere in the retina, there is a stress response (Fig. 5E-H, Supplementary Fig. S7A-D). We also stained for F4/80, a marker for macrophages/microglia. In the mutant retinas positive staining was found in the interior of retinal folds but not elsewhere in the photoreceptor layer (Fig. 5J-L, Supplementary Fig. S7E-H). The amoeboid shape of the positively-stained cells suggests that they are macrophages that have infiltrated into the retinal folds containing excess and disorganised outer segments and that they are phagocytosing degenerating outer segments. We did not observe melanin within the macrophages indicating that they had not engulfed pigmented RPE cells. Finally we examined by transmission electron microscopy the ultrastructural architecture of the boundary between the RPE and outer segments (Fig. 6). For the homozygous mutants, in retinal areas without folds, the boundary between outer segments and RPE appeared normal (compare Fig. 6A with Fig. 6B and D). However, in the areas with folds the outer segments were disorganised and appeared to be degenerating, with cavitites and other celluar debris apparent (Fig. 6C and 6E).

DISCUSSION

Rwhs is Caused by a Missense Mutation in *Tmem98* that is Homozygous Lethal

Here we report that the ENU-induced dominant retinal white spotting phenotype, *Rwhs*, is caused by an I135T missense mutation in the highly conserved transmembrane protein encoding gene *Tmem98*. We also found that when homozygous the *Tmem98*^{I135T} allele is perinatally lethal. *Tmem98* was one of the genes included in an international project to produce and phenotype knockout mouse lines for 20,000 genes [41]. The targeted allele, *Tmem98*^{tm1a}, was subjected to a high-content phenotyping pipeline (results available at http://www.mousephenotype.org/data/genes/MGI:1923457). It was found to be lethal pre-weaning as homozygotes, but no significant heterozygous phenotypic variation from wild-type was reported. Neither their slit lamp analysis nor our retinal examination found any eye defects in knock-out heterozygous mice. We also found that *Tmem98*^{tm1a} is homozygous lethal and narrowed the stage of lethality to the perinatal stage (Table S1). This suggests that haploinsufficency for TMEM98 protein does not cause a retinal phenotype and that the I135T mutation in TMEM98 is not a loss-of-function allele but changes the protein's function leading to the retinal white spotting phenotype.

Phenotype of Human Nanophthalmos Associated *TMEM98* Missense Mutations in the Mouse

Tmem98 has been previously suggested to be a novel chemoresistance-conferring gene in hepatoceullular carcinoma [42]. It has also been reported to be able to promote the differentiation of T helper 1 cells and to be involved in the invasion and migration of lung cancer cells [39, 43]. Recently it has been reported that TMEM98 interacts with MYRF and prevents its autocatalytic cleavage [44]. In relation to human disease two TMEM98 missense mutations, A193P and H196P, have been reported to be associated with dominant nanophthalmos [21, 22]. We introduced these mutations into the mouse gene and found that mice homozygous for either, or compound heterozygous for both, developed white patches on their retinas accompanied by retinal folds, replicating the dominant phenotype found in the ENU-induced allele. We also observed for all three alleles separation of the RPE away from the neural retina in the areas under the folds. Mice lacking *Tmem98* do not survive after birth (Supplementary Table S2). The three missense mutations described here are not null.

The two human mutations are homozygous viable, and the mouse mutation, when in combination with a knock-out allele is also viable (data not shown). Furthermore, the H196P missense mutation in combination with a gene knockout has no detectable eye phenotype and the mice are viable (Supplementary Fig. S6). This indicates that the recessive mutations are not loss of function, but are gain of function with, in the case of H196P at least, a threshold dosage requirement. However, the phenotypes are different from the reported dominant nanophthalmos caused by the same mutations in humans.

Other genes causing nanophthalmos may also be gain of function. The serine protease *PRSS56* is a recessive posterior microphthamia or nanophthalmos mutant gene in humans, with both identified mutations affecting the C-terminus of the protein [17]. The mouse mutant model of this gene, which produces a variable and slight reduction in ocular length, is a splice site mutation resulting in a truncated protein which nevertheless has normal protease activity *in vitro* [17]. Recently the phenotype of a null allele of *Prss56* has been described and it does cause some reduction in ocular size and hyperopia [34].

The mouse model of the nanophthalmos gene, *Mfrp*, does not reproduce the human phenotype. Rather, loss of function of this gene results in white spots apparent on retinal imaging (retinitis punctata albicans) but these have different origin from the phenotype we observe, and progress to photoreceptor degeneration. It has been reported that the *Mfrp* knockout mice have eyes that are slightly (but not statistically significantly) smaller, by about 2% in axial length. It is worth noting that different strains of mice have measurably different ocular size. Strain differences of up to 2% and sex differences of over 1.5% have been reported [45].

Two genes that are infrequently associated with nanopthalmos, *CRB1* and *BEST1*, both can produce a mouse phenotype apparently indistinguishable from the one we describe here. Furthermore, the knockout mouse model of the nuclear receptor gene, *Nrl*, also develops retinal rosettes during post-natal life [46]. The *Nrl* mutant eye has defects in the outer limiting membrane (OLM), a component of which is the CRB1 protein. The *Tmem98* mutations have OLM defects, but we cannot ascertain whether these defects are the primary cause of the folds or a secondary consequence.

Retinal folds are a characteristic of nanophthalmic eyes and this is usually attributed to a differential growth of neural retina within the smaller optic cup. Our data show that folds can be seen in a normal-sized eye, but we do not know whether there is nevertheless excess

growth of the neural retina. The retinal defects we see are not associated with an ERG deficit, suggesting that the rest of the retina, unaffected by the folds, is functionally normal.

Notable is the detachment of the retina from the RPE within the folds (rosettes). In the *Nrl* and *Crb1* mutant eyes the photoreceptors that have lost their connection to the RPE can be seen to degenerate. We see no evidence of photoreceptor degeneration in the *Tmem98* mutants. The mechanism of the pathology is still unclear. As *Tmem98* is strongly expressed in the RPE, and not at all in the photoreceptors, it is likely that RPE is the affected tissue. The key observation in these and other mouse models of nanophthalmos is that the defects are focal and progressive, suggesting that secondary events exacerbate an underlying but (given ERG data) non-pathological defect. The accumulation of photoreceptor cell debris below the retinal folds suggests a focal defect in outer segment phagocytosis but one that does not lead to photoreceptor degeneration. Three of the genes associated with nanophthalmos are expressed in the RPE; *Tmem98*, *Best1* and *Myrf*. *Crb1* is expressed in photoreceptors and *Prss56*, a secreted serine protease, is expressed in the Müller cells. It is possible that these genes interact and affect a common pathway, indeed upregulation of *Prss56* has been observed in *Mfrp* mutants [47]. The recent finding that TMEM98 binds to and prevents the activation of the oligodendrocyte transcription factor MYRF (also highly expressed in the RPE; http://www.biogps.org) will perhaps lead to a mechanistic explanation [44].

Acknowledgements

We thank Morag Robertson for help with genotyping, Craig Nicol and Connor Warnock for help with photography, the IGMM Advanced Imaging Resource for help with imaging and MRC Human Genetics Unit scientific support services.

References

1. Verma AS, FitzPatrick DR. Anophthalmia and microphthalmia. *Orphanet journal of rare diseases* 2007;2:47.
2. Carricondo PC, Andrade T, Prasov L, Ayres BM, Moroi SE. Nanophthalmos: A Review of the Clinical Spectrum and Genetics. *Journal of ophthalmology* 2018;2018.
3. Boon CJ, Klevering BJ, Leroy BP, Hoyng CB, Keunen JE, den Hollander AI. The spectrum of ocular phenotypes caused by mutations in the BEST1 gene. *Progress in retinal and eye research* 2009;28:187-205.
4. Marmorstein AD, Marmorstein LY, Rayborn M, Wang X, Hollyfield JG, Petrukhin K. Bestrophin, the product of the Best vitelliform macular dystrophy gene (VMD2), localizes to the

basolateral plasma membrane of the retinal pigment epithelium. *Proceedings of the National Academy of Sciences* 2000;97:12758-12763.
5. Petrukhin K, Koisti MJ, Bakall B, et al. Identification of the gene responsible for Best macular dystrophy. *Nature genetics* 1998;19:241.
6. Yardley J, Leroy BP, Hart-Holden N, et al. Mutations of VMD2 splicing regulators cause nanophthalmos and autosomal dominant vitreoretinochoroidopathy (ADVIRC). *Investigative ophthalmology & visual science* 2004;45:3683-3689.
7. Pellikka M, Tanentzapf G, Pinto M, et al. Crumbs, the Drosophila homologue of human CRB1/RP12, is essential for photoreceptor morphogenesis. *Nature* 2002;416:143.
8. den Hollander AI, Jacoline B, de Kok YJ, et al. Mutations in a human homologue of Drosophila crumbs cause retinitis pigmentosa (RP12). *Nature genetics* 1999;23:217.
9. den Hollander AI, Heckenlively JR, van den Born LI, et al. Leber congenital amaurosis and retinitis pigmentosa with Coats-like exudative vasculopathy are associated with mutations in the crumbs homologue 1 (CRB1) gene. *The American Journal of Human Genetics* 2001;69:198-203.
10. Zenteno JC, Buentello-Volante B, Ayala-Ramirez R, Villanueva-Mendoza C. Homozygosity mapping identifies the Crumbs homologue 1 (Crb1) gene as responsible for a recessive syndrome of retinitis pigmentosa and nanophthalmos. *American Journal of Medical Genetics Part A* 2011;155:1001-1006.
11. Paun CC, Pijl BJ, Siemiatkowska AM, et al. A novel crumbs homolog 1 mutation in a family with retinitis pigmentosa, nanophthalmos, and optic disc drusen. *Molecular vision* 2012;18:2447.
12. Sundin OH, Leppert GS, Silva ED, et al. Extreme hyperopia is the result of null mutations in MFRP, which encodes a Frizzled-related protein. *Proceedings of the National Academy of Sciences* 2005;102:9553-9558.
13. Ayala-Ramirez R, Graue-Wiechers F, Robredo V, Amato-Almanza M, Horta-Diez I, Zenteno JC. A new autosomal recessive syndrome consisting of posterior microphthalmos, retinitis pigmentosa, foveoschisis, and optic disc drusen is caused by a MFRP gene mutation. *Molecular vision* 2006;12:1483-1489.
14. Zenteno JC, Buentello-Volante B, Quiroz-González MA, Quiroz-Reyes MA. Compound heterozygosity for a novel and a recurrent MFRP gene mutation in a family with the nanophthalmos-retinitis pigmentosa complex. *Molecular vision* 2009;15:1794.
15. Neri A, Leaci R, Zenteno JC, Casubolo C, Delfini E, Macaluso C. Membrane frizzled-related protein gene–related ophthalmological syndrome: 30-month follow-up of a sporadic case and review of genotype-phenotype correlation in the literature. *Molecular vision* 2012;18:2623.
16. Gal A, Rau I, El Matri L, et al. Autosomal-recessive posterior microphthalmos is caused by mutations in PRSS56, a gene encoding a trypsin-like serine protease. *The American Journal of Human Genetics* 2011;88:382-390.
17. Nair KS, Hmani-Aifa M, Ali Z, et al. Alteration of the serine protease PRSS56 causes angle-closure glaucoma in mice and posterior microphthalmia in humans and mice. *Nature Genetics* 2011;43:579.
18. Orr A, Dubé M-P, Zenteno JC, et al. Mutations in a novel serine protease PRSS56 in families with nanophthalmos. *Molecular vision* 2011;17:1850.
19. Kiefer AK, Tung JY, Do CB, et al. Genome-wide analysis points to roles for extracellular matrix remodeling, the visual cycle, and neuronal development in myopia. *PLoS genetics* 2013;9:e1003299.
20. Verhoeven VJ, Hysi PG, Wojciechowski R, et al. Genome-wide meta-analyses of multiancestry cohorts identify multiple new susceptibility loci for refractive error and myopia. *Nat Genet* 2013;45:314-318.
21. Awadalla MS, Burdon KP, Souzeau E, et al. Mutation in TMEM98 in a large white kindred with autosomal dominant nanophthalmos linked to 17p12-q12. *JAMA ophthalmology* 2014;132:970-977.

480 22. Khorram D, Choi M, Roos BR, et al. Novel TMEM98 mutations in pedigrees with autosomal
481 dominant nanophthalmos. *Molecular vision* 2015;21:1017-1023.
482 23. Sun W, Zhang Q. Does the association between TMEM98 and nanophthalmos require
483 further confirmation? *JAMA ophthalmology* 2015;133:358-359.
484 24. Marmorstein LY, Wu J, McLaughlin P, et al. The light peak of the electroretinogram is
485 dependent on voltage-gated calcium channels and antagonized by bestrophin (best-1). *The Journal*
486 *of general physiology* 2006;127:577-589.
487 25. Milenkovic A, Brandl C, Milenkovic VM, et al. Bestrophin 1 is indispensable for volume
488 regulation in human retinal pigment epithelium cells. *Proceedings of the National Academy of*
489 *Sciences* 2015;112:E2630-E2639.
490 26. Zhang Y, Stanton JB, Wu J, et al. Suppression of Ca 2+ signaling in a mouse model of Best
491 disease. *Human molecular genetics* 2010;19:1108-1118.
492 27. Mehalow AK, Kameya S, Smith RS, et al. CRB1 is essential for external limiting membrane
493 integrity and photoreceptor morphogenesis in the mammalian retina. *Human molecular genetics*
494 2003;12:2179-2189.
495 28. van de Pavert SA, Kantardzhieva A, Malysheva A, et al. Crumbs homologue 1 is required for
496 maintenance of photoreceptor cell polarization and adhesion during light exposure. *Journal of Cell*
497 *Science* 2004;117:4169-4177.
498 29. van de Pavert SA, Meuleman J, Malysheva A, et al. A single amino acid substitution
499 (Cys249Trp) in Crb1 causes retinal degeneration and deregulates expression of pituitary tumor
500 transforming gene Pttg1. *Journal of Neuroscience* 2007;27:564-573.
501 30. Kameya S, Hawes NL, Chang B, Heckenlively JR, Naggert JK, Nishina PM. Mfrp, a gene
502 encoding a frizzled related protein, is mutated in the mouse retinal degeneration 6. *Human*
503 *molecular genetics* 2002;11:1879-1886.
504 31. Fogerty J, Besharse JC. 174delG mutation in mouse MFRP causes photoreceptor
505 degeneration and RPE atrophy. *Investigative ophthalmology & visual science* 2011;52:7256-7266.
506 32. Hawes NL, Chang B, Hageman GS, et al. Retinal degeneration 6 (rd6): a new mouse model for
507 human retinitis punctata albescens. *Investigative ophthalmology & visual science* 2000;41:3149-
508 3157.
509 33. Velez G, Tsang SH, Tsai Y-T, et al. Gene Therapy Restores Mfrp and Corrects Axial Eye Length.
510 *Scientific Reports* 2017;7:16151.
511 34. Paylakhi S, Labelle-Dumais C, Tolman NG, et al. Muller glia-derived PRSS56 is required to
512 sustain ocular axial growth and prevent refractive error. *PLoS Genet* 2018;14:e1007244.
513 35. Thaung C, West K, Clark BJ, et al. Novel ENU-induced eye mutations in the mouse: models
514 for human eye disease. *Human molecular genetics* 2002;11:755-767.
515 36. White JK, Gerdin A-K, Karp NA, et al. Genome-wide generation and systematic phenotyping
516 of knockout mice reveals new roles for many genes. *Cell* 2013;154:452-464.
517 37. Skarnes WC, Rosen B, West AP, et al. A conditional knockout resource for the genome-wide
518 study of mouse gene function. *Nature* 2011;474:337.
519 38. Cong L, Ran FA, Cox D, et al. Multiplex genome engineering using CRISPR/Cas systems.
520 *Science* 2013;1231143.
521 39. Fu W, Cheng Y, Zhang Y, et al. The Secreted Form of Transmembrane Protein 98 Promotes
522 the Differentiation of T Helper 1 Cells. *Journal of interferon & cytokine research : the official journal*
523 *of the International Society for Interferon and Cytokine Research* 2015;35:720-733.
524 40. Lewis GP, Fisher SK. Up-regulation of glial fibrillary acidic protein in response to retinal
525 injury: its potential role in glial remodeling and a comparison to vimentin expression. *International*
526 *review of cytology* 2003;230:264-290.
527 41. Brown SD, Holmes CC, Mallon A-M, Meehan TF, Smedley D, Wells S. High-throughput mouse
528 phenomics for characterizing mammalian gene function. *Nature Reviews Genetics* 2018;1.

529 42. Ng KT, Lo CM, Guo DY, et al. Identification of transmembrane protein 98 as a novel
530 chemoresistance-conferring gene in hepatocellular carcinoma. *Molecular cancer therapeutics*
531 2014;13:1285-1297.
532 43. Mao M, Chen J, Li X, Wu Z. siRNA-TMEM98 inhibits the invasion and migration of lung cancer
533 cells. *International journal of clinical and experimental pathology* 2015;8:15661-15669.
534 44. Huang H, Teng P, Du J, et al. Interactive repression of MYRF self-cleavage and activity in
535 oligodendrocyte differentiation by TMEM98 protein. *The Journal of neuroscience : the official journal*
536 *of the Society for Neuroscience* 2018.
537 45. Puk O, de Angelis MH, Graw J. Longitudinal fundus and retinal studies with SD-OCT: a
538 comparison of five mouse inbred strains. *Mamm Genome* 2013;24:198-205.
539 46. Haider NB, Naggert JK, Nishina PM. Excess cone cell proliferation due to lack of a functional
540 NR2E3 causes retinal dysplasia and degeneration in rd7/rd7 mice. *Human molecular genetics*
541 2001;10:1619-1626.
542 47. Soundararajan R, Won J, Stearns TM, et al. Gene profiling of postnatal Mfrprd6 mutant eyes
543 reveals differential accumulation of Prss56, visual cycle and phototransduction mRNAs. *PloS one*
544 2014;9:e110299.

545

546 Tables

547 Table 1. Sequences of oligos

Oligo Name	Sequence (5'-3')*
ex7_Guide1	CACCGGCCAATCACTGTCTGCCGCTG
ex7_Guide2	AAACCAGCGGCAGACAGTGATTGGCC
A193P	AACCGCCCTGCTGCTGTCCGTTAGTCACTTGGTGCTAGTGACCAGGA ACGCCTGCCATCTAACCGGGGGCCTGGACTGGATTGACCAATCACT GTCTGCCCCTGAAGAGCACCTGGAAGTCCTTCGAGAGGCAGCCCTG GCTTCTGAGCCAGATAAAAGCCTCCCCAACCCTGAGGGCTTCCTGCA GGAACAGTCGGCCA
H196P	AACCGCCCTGCTGCTGTCCGTTAGTCACTTGGTGCTAGTGACCAGGA ACGCCTGCCATCTAACCGGGGGCCTGGACTGGATTGACCAATCACT GTCTGCCGCTGAAGAGCCCCTGGAAGTCCTTCGAGAGGCAGCCCTG GCTTCTGAGCCAGATAAAAGCCTCCCCAACCCTGAGGGCTTCCTGCA GGAACAGTCGGCCA

548 *For the repair oligos base changes introducing amino acid changes are highlighted in red
549 and silent base changes destroying the PAM site are highlighted in blue. In the A193P line
550 only the mutation causing the A193P change was found, in the H196P line both base
551 changes were incorporated.

552

553 **Table 2. Primary antibodies**

Antibody	Source	Product No	Concentration used
anti-TMEM98	proteintech	14731-1-AP	1:5000 (WB), 1:100 (IF)
anti-α-Tubulin	Sigma-Aldrich	T5168	1:10,000 (WB)
anti-Prominin 1	proteintech	18470-1-AP	1:100 (IF)
anti-Rhodopsin	Millipore	MAB5356	1:500 (IF)
anti-ML Opsin	Millipore	AB5405	1:500 (IF)
anti-GFAP	abcam	ab7260	1:500 (IF)
anti-β-Catenein	Cell Signaling Technology	19807S	1:500 (IF)
Anti-F4/80	AbD Serotec	MCA497EL	1:500 (IF)

554 Key: WB=Western blotting, IF=immunofluorescence

555

556 **Table 3. *Tmem98*$^{Rwhs/+}$ intercross genotyping results**

Age	WT	*Rwhs*/+	*Rwhs/Rwhs*	Total	P*
adult	34	79	0	113	<0.0001
E17.5-E18.5	2	12	5	19	0.3225

557 *Test for significance using chi-square test

Figures

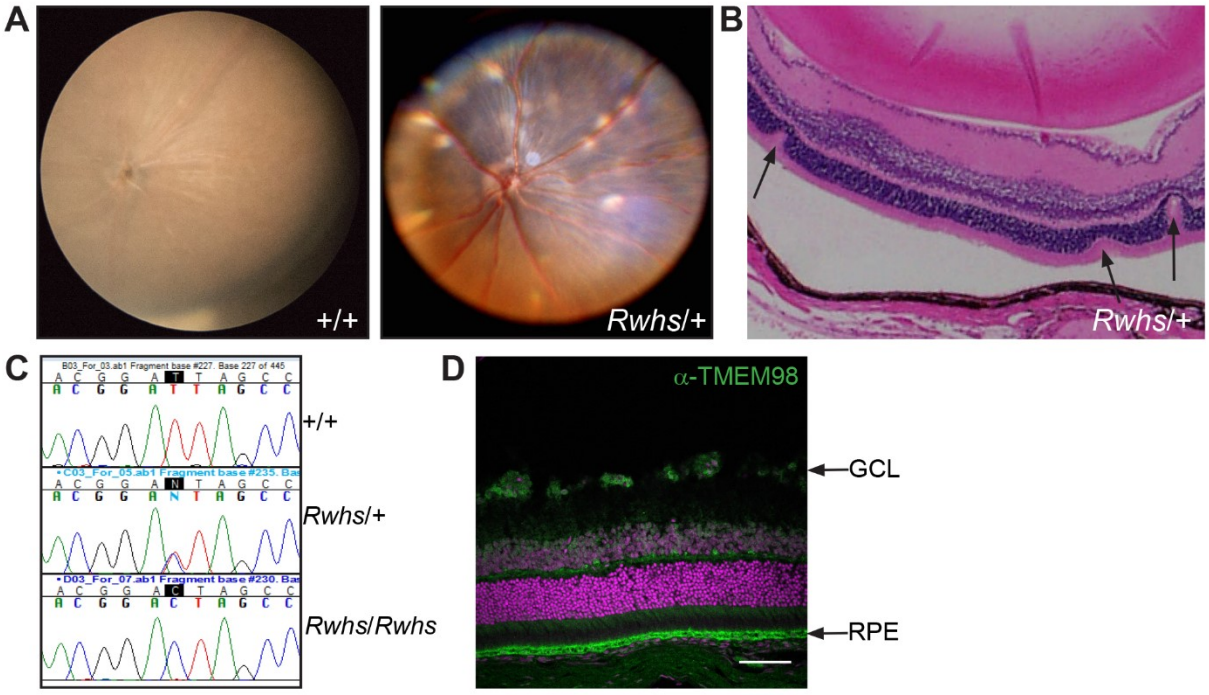

Figure 1. The *Rwhs* mutation is caused by an I135T mutation of the transmembrane gene *Tmem98*. (**A**) Retinal images of wild-type (+,+) and *Rwhs*/+ eyes. Scattered white spots are present on the *Rwhs*/+ retina. (**B**) *Rwhs*/+ retinal section with three folds in the outer nuclear layer indicated by arrows. (**C**) Genomic DNA sequence traces from exon 5 of *Tmem98* from wild-type (+/+), heterozygous mutant (*Rwhs*/+) and homozygous mutant (*Rwhs*/*Rwhs*) embryonic samples. The position of the T-to-C transition at position 404 (404T>C) in *Tmem98* is highlighted. (**D**) A section of wild-type retina immunostained for TMEM98 (green). Prominent staining is seen in the retinal pigment epithelium (RPE) and there is also some staining in the ganglion cell layer (GCL). DNA is shown in magenta. Scale bar: 100 μM (**D**).

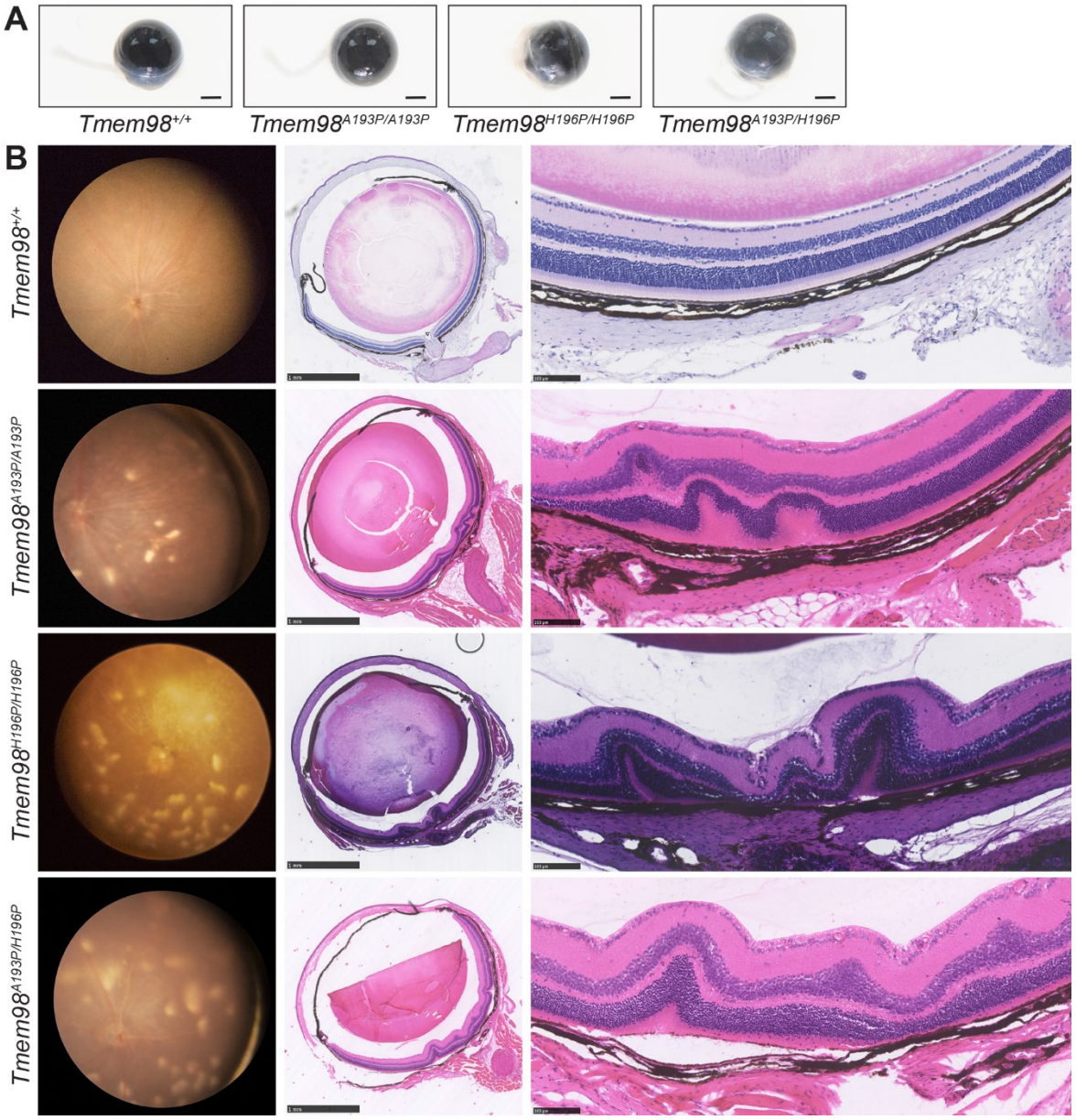

Figure 2. Whole eye and retinal phenotypes of homozygous and compound heterozygous mice with human nanophthalmos missense mutations. (**A**) Pictures of eyes from wild-type and mutant mice. The eyes of the homozygous and compound heterozygous mutants are not noticeably smaller than the wild-type eye. (**B**) Left panel, retinal images; centre panel sections through the optic nerve; right panel, higher magnification pictures of the retina. *Tmem98*$^{A193P/A193P}$, *Tmem98*$^{H196P/H196P}$ and *Tmem98*$^{A193P/H196P}$ retinas all have scattered white spots (left panel) and folds in the outer nuclear layer and sometimes the inner retinal layers as well (centre and right panels). Scale bars: 1 mm (**A** and **B**, centre panel), 100 μM (**B**, right panel).

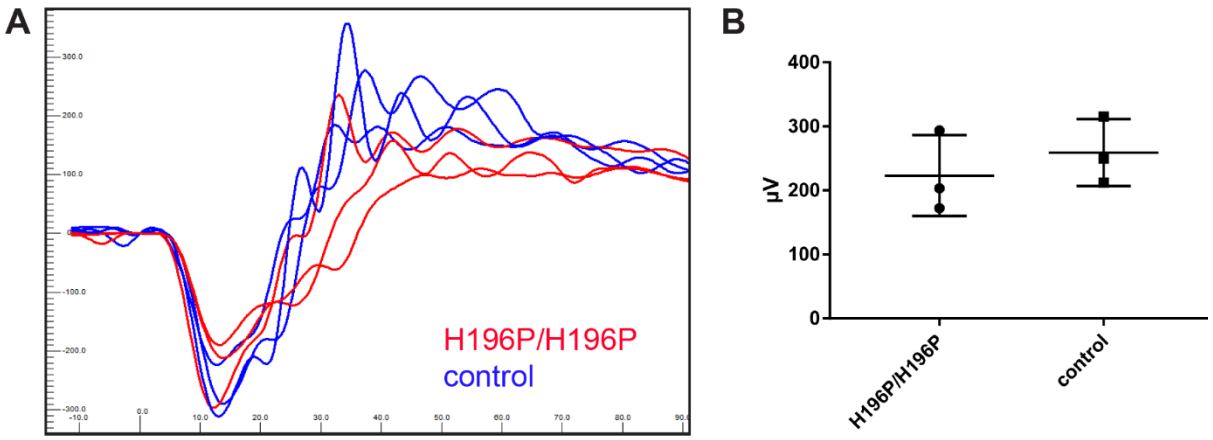

Figure 3. *Tmem98*$^{H196P/H196P}$ mice have a normal ERG response. Three *Tmem98*$^{H196P/H196P}$ mice and three control mice (two wild-type and one *Tmem98*$^{H196P/+}$) were tested at 6 months of age. (**A**) ERG traces of *Tmem98*$^{H196P/H196P}$ mice (red lines), and control mice (blue lines). Shown are the responses at 3 cd.s/m^2 (average of 4 flashes) for the left eye. (**B**) Comparison of a-wave amplitudes, average of left and right eye for each mouse. There is no significant difference between *Tmem98*$^{H196P/H196P}$ and control (unpaired t test with Welch's correction, P = 0.81).

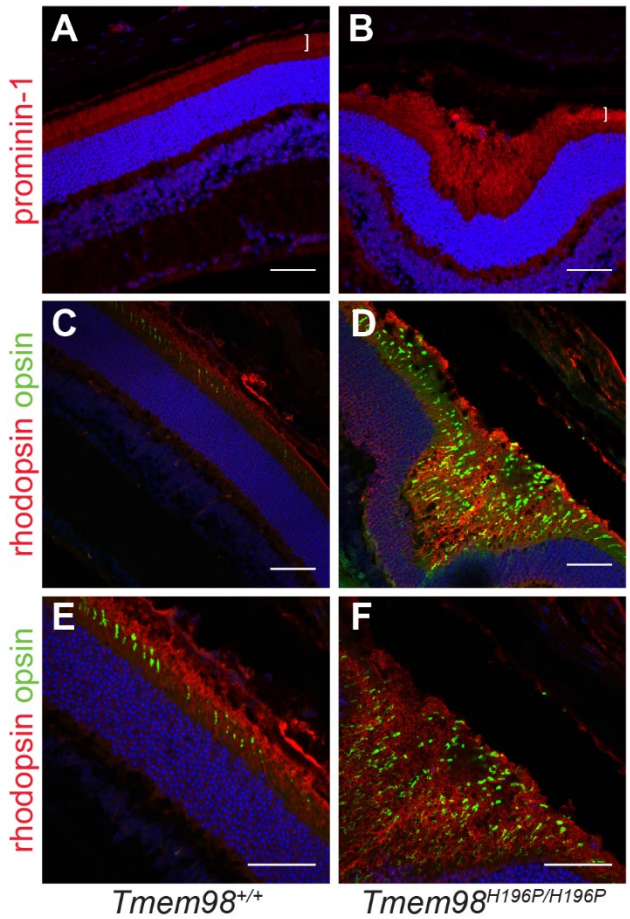

589

590 **Figure 4.** The interiors of the retinal folds found in the *Tmem98*$^{H196P/H196P}$ mutant mice are
591 filled with excess outer segments. Immunostaining of retinal sections from wild-type mice (**A**,
592 **C** and **E**) and *Tmem98*$^{H196P/H196P}$ mice (**B**, **D** and **F**). (**A**-**B**) Prominin-1 staining (red) shows
593 that the outer segment layer (white bracket) is expanded in the retinal fold of the mutant (**B**)
594 compared to wild-type (**A**). (**C**-**F**) Rhodopsin (red) and opsin (green) staining shows that the
595 interior of the retinal fold is filled with outer segments. DAPI staining is shown in blue. Scale
596 bars: 50 μM.

597

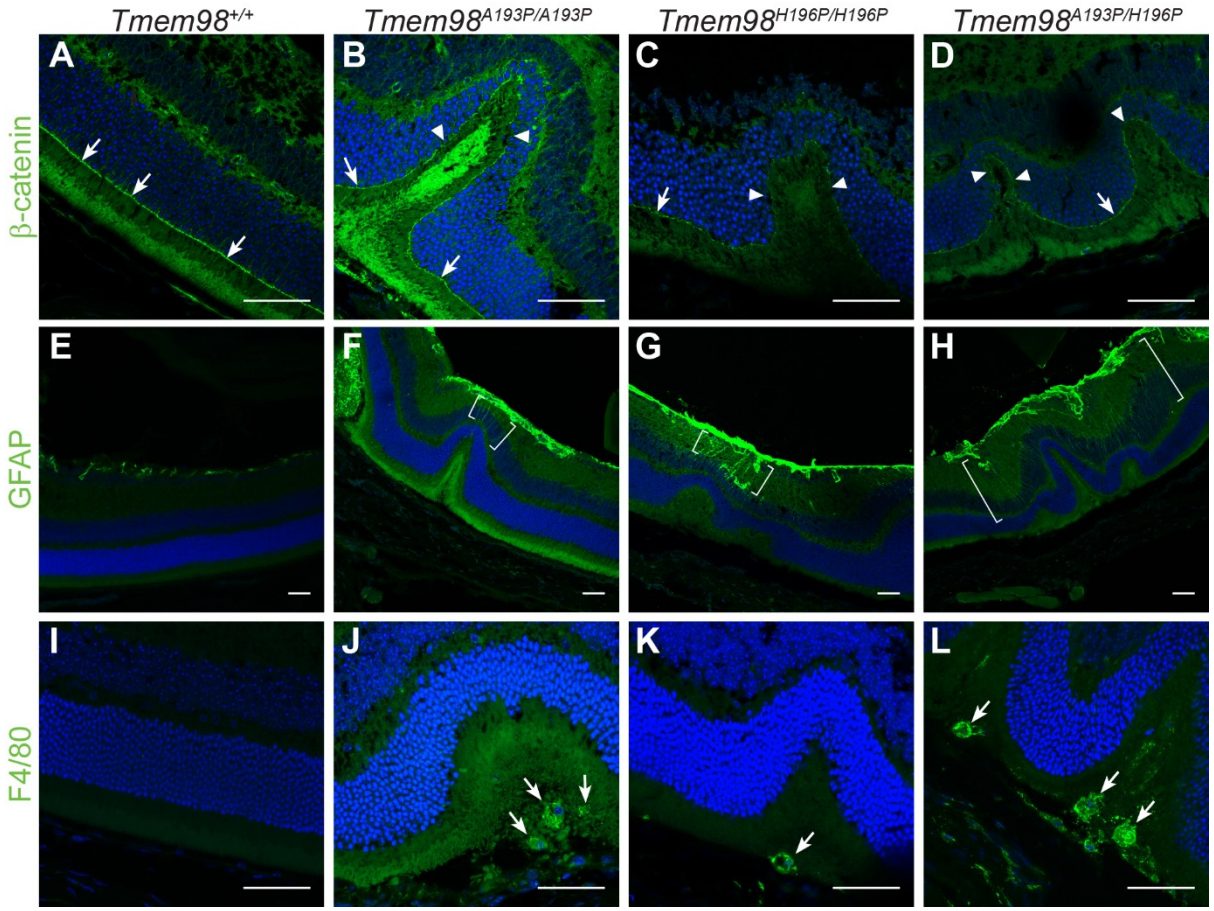

Figure 5. Characterisation of the retinal folds in the *Tmem98* mutant mice. Immunostaining of retinal sections from wild-type mice (**A**, **E** and **I**), *Tmem98*$^{A193P/A193P}$ mice (**B**, **F** and **J**), *Tmem98*$^{H196P/H196P}$ mice (**C**, **G** and **K**), *Tmem98*$^{A193P/H196P}$ mice (**D**, **H** and **L**). (**A-D**) β-catenin staining (green) shows that the OLM is intact in the wild-type retina and in the areas either side of folds in the mutant retinas (white arrows) but in the folds of the mutant retinas the OLM is interrupted (white arrowheads). (**E-H**) GFAP staining (green) is normal in the wild-type retina but above the folds in the mutant retinas there is abnormal GFAP staining extending towards the outer nuclear layer (areas between the white brackets). This indicates that in the mutants the retina is stressed in the folded regions and that retinal stress is confined to the folds. (**I-L**) F4/80 staining (green) reveals that macrophages have infiltrated into the areas below the folded outer nuclear layer containing excess photoreceptors in the mutant retinas (white arrows). Staining was not observed outside the folds in the mutant retinas. DAPI staining is shown in blue. Scale bars: 50 μm.

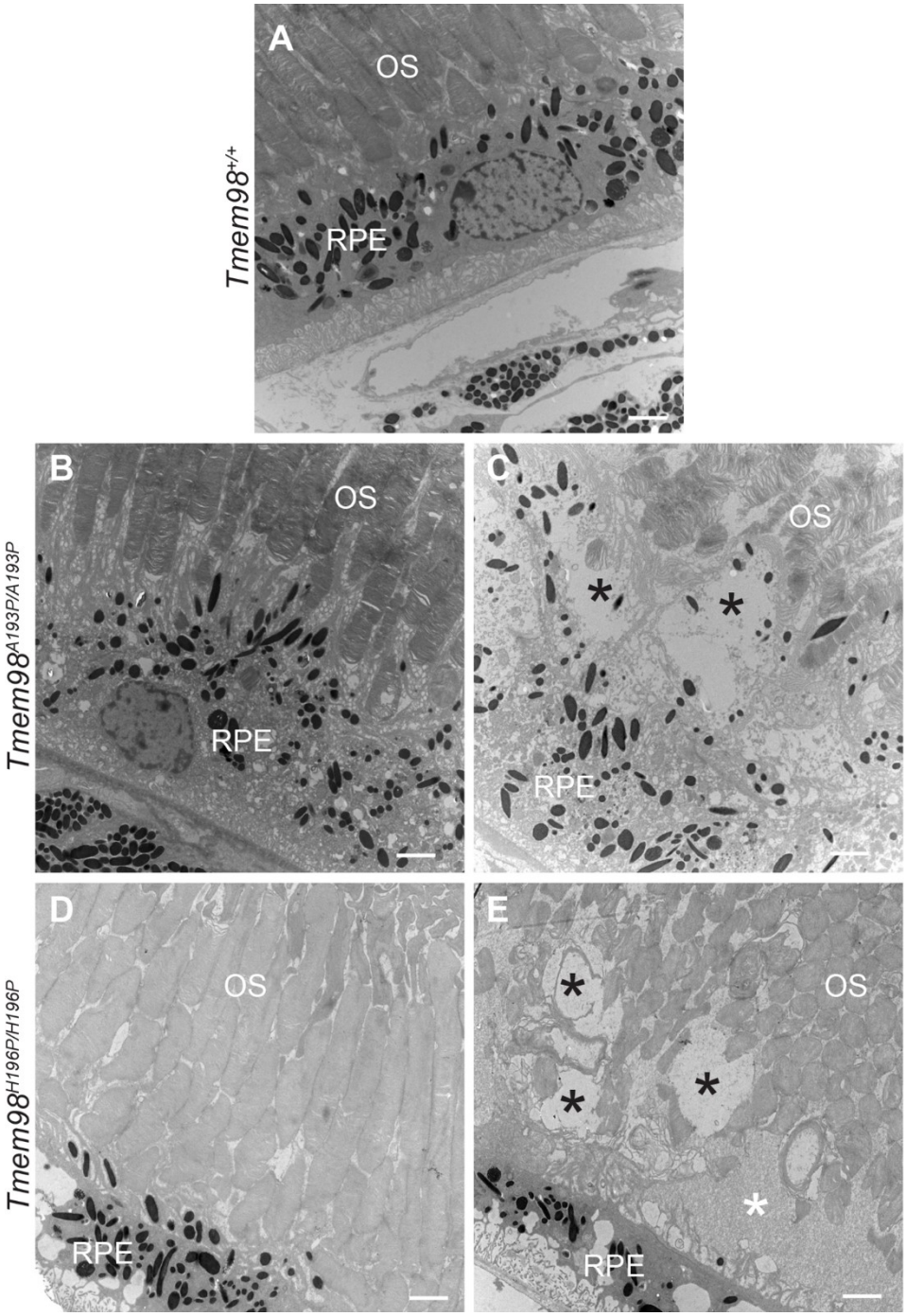

Figure 6. Ultrastructural analysis of the RPE and outer segment boundary. (**A**) Wild-type mice are normal. (**B** and **D**) In mutant mice from retinal regions with no folds the outer segments adjacent to the RPE appear normal. (**C** and **E**) In retinal areas with folds the outer segments abutting the RPE appear abnormal and disorganised. Several large vacuoles (indicated by black asterisks) can be seen. In (**E**) there is an area containing cellular debris (indicated by a white asterisk). *Tmem98*$^{A193P/A193P}$ (**B**, **C**) and *Tmem98*$^{H196P/H196P}$ (**D**, **E**). OS = outer segments, RPE = retinal pigment epithelium. Scale bars: 2μm.